ELSEVIER

International Journal of Heat and Fluid Flow 22 (2001) 245–251

International Journal of HEAT AND FLUID FLOW

www.elsevier.com/locate/ijhff

Direct numerical simulation of carbon-dioxide gas absorption caused by turbulent free surface flow

Tomoaki Kunugi [a,*], Shin-ichi Satake [b], Yasuo Ose [c]

[a] *Department of Nuclear Engineering, Kyoto University, Yoshida, Sakyo, Kyoto 606-8501, Japan*
[b] *Department of Mechanical and Intellectual Systems Engineering, Toyama University, 3190 Gofuku, Toyama 930-8555, Japan*
[c] *Department of System Engineering, Yamato System Engineering, Co. Ltd., Hitachi, Ibaraki 317, Japan*

Abstract

The turbulent behavior of liquid and gas flows at a free surface is not very well understood in comparison with that of the motions at the solid boundary. In the present study, the DNS for the turbulent free surface flow with a shear wind has been carried out by means of a coupled gas–liquid flow solution procedure, i.e., multi-interface and advection and reconstruction solver (MARS) developed by one of the authors. Henry's law is applied to the evaluation of a saturated gas concentration at the free surface caused by the carbon-dioxide gas absorption. Resulting from the present DNS of turbulent free surface flow with carbon-dioxide gas transfer at the gas–water interface, the mean and root-mean-square distributions of velocity, pressure and concentration and their fluctuations throughout both the gas and liquid flow fields are obtained and compared with the experimental data. Finally, an exchange coefficient of carbon-dioxide gas at the turbulent free surface estimated in this study is in good agreement with the existing experimental and sea-measurement data.

Keywords: Turbulent free surface flow; Carbon-dioxide gas absorption; Air–water interaction; Gas exchange coefficient; Direct numerical simulation

1. Introduction

The turbulent behavior of liquid and gas flows at a free surface is not very well understood in comparison with that of the motions at the solid boundary. However, turbulent behaviors of both free surface and solid wall cases are equally important in the practical application. In addition, the mechanism of scalar transport into a turbulent liquid flows across the gas–liquid interfaces or free surfaces is of great importance in the industrial devices, especially a chemical process like gas-absorption equipment and so on. Recently, the turbulent mass transport of the carbon-dioxide is very important for the global warming because of understanding the "Missing sink" due to a mass imbalance of the carbon production and consumption by human beings after the industrial revolution.

There are many studies on the liquid-side turbulence near the free surface imposed with zero or very low shear flow (Rashidi and Banerjee, 1988; Komori et al., 1989). In case of the low wind velocity, most of the previous studies have considered that the turbulence structure is generated by the shear rate in the liquid-side flow rather than by the coupling effect between the gas- and liquid-flows. However, in case of the capillary and capillary-gravity range wind velocity, i.e., around 2–7 m/s, the turbulent characteristics near the free surface could be influenced by a deformation of the free surface due to the shear wind.

A few direct numerical simulations (DNSs) and experimental investigations for the turbulent free surface flows have been carried out because of the numerical and experimental difficulties in numerical tracking/capturing and experimental measurement of the transient deformation of the free surface. Recently, DNS with coupling procedure of gas–liquid interaction was performed by Lombardi et al. (1996). However, they still assumed that the interface was kept flat, i.e., this assumption was similar to the previous study (Lam and Banerjee, 1992). Angelis and Banerjee (1999) focused on the capillary and capillary-gravity range wind velocity and presented some correlation between mass flux and turbulent structure. Although their surface can be deformed by the shear wind, the interface momentum and continuity treatments are almost the same as Lombardi et al. (1996). Another free surface treatment by Tsai (1998) was linearized by assuming a free surface deformation of $\varepsilon \sim \mathrm{O}(Fr)$ and a free surface boundary layer thickness $\delta \sim \mathrm{O}(Re^{-1/2})$, with $\delta^2 \ll \varepsilon \ll \delta \ll 1$. Here, Reynolds number is based on the shear layer thickness h, the free-stream velocity U_∞ and kinematic viscosity of bulk fluid v and Froude number $Fr = U_\infty/(gh)^{1/2}$, where g is the gravitational acceleration. However, most of the liquid surfaces are treated like a solid wall boundary condition. These treatments

* Corresponding author. Tel.: +81-75-753-5823; fax: +81-75-753-5823.
E-mail address: kunugi@nucleng.kyoto-u.ac.jp (T. Kunugi).

0142-727X/01/$ - see front matter
PII: S0142-727X(01)00086-8

Notation

C	concentration (molar fraction)
C_s	saturated concentration at free surface
D	molecular diffusivity
D_{turb}	turbulent diffusivity
E_C	energy spectra of concentration
E_F	energy spectrum of F function
E_{ii}	energy spectrum of ith velocity component
F	volume of fluid function
F_m	F of the mth fluid
Fr	Froude number
F_v	CSF term for surface tension
G	gravity term
H	Henry's coefficient
h	gas/liquid layer height in solution domain
J	turbulent exchange molar flux in y-direction
k_L	gas exchange coefficient
k_x	wave number in streamwise direction
L	streamwise length of solution domain
L_x	wavelength in streamwise direction
n	normal vector to free surface
P	pressure
P_s	pressure at free surface
Re	Reynolds number $= U_\infty h/\nu$
Re_τ	turbulent Reynolds number $= u_\tau h/\nu$
S	absorbed mass flux of carbon-dioxide gas
t	time
$U,\ V,\ W$	velocity vector
U_∞	free-stream velocity
$u_{rms},\ v_{rms},\ w_{rms}$	root-mean-square of velocity fluctuation for $U,\ V,\ W$, respectively
$u',\ v',\ w'$	velocity fluctuation
W	spanwise length of solution domain
x_i	coordinate of the ith direction
x_s	free surface position

Greek

δ	boundary layer thickness
ε	free surface deformation
ϕ	general variables
κ	curvature
μ	viscosity
ν	kinetic viscosity
ρ	density
σ	surface tension
τ	shear stress

Subscripts

$(\ )_g$	gas phase
$(\ )_l$	liquid phase

will have to meet the essential difficulty when the liquid surface breaks due to a high shear flow.

On the other hand, in order to understand the gas–liquid interaction at the turbulent free-surface for higher velocity range, the authors have been developing a precise free-surface capturing algorithm for two-phase flows, i.e., multi-interface advection and reconstruction solver (MARS) (Kunugi, 1997), and provided a high-quality initial turbulent field for both gas- and liquid-flows via a time-dependent three-dimensional DNS (Satake and Kunugi, 1998). Moreover, we have been investigating the turbulent scalar transport from the air to the sea due to the strong interaction between liquid and gas (Kunugi et al., 1999a,b). However, in our previous study the potential of the MARS to solve the multi-phase flows was only emphasized and the preliminary DNS results were shown.

In the present study, DNS of turbulent free-surface flow with the relatively low shear wind (around $U_\infty = 2.15$ m/s) has been carried out by means of the coupled gas–liquid flow solution procedure (MARS). Resulting from the present DNS of turbulent free surface flow with carbon-dioxide gas transfer at the gas–water interface, mean and root-mean-square distributions regarding the velocity, pressure and concentration and their fluctuations throughout both the gas and liquid flow fields are obtained. Finally, exchange coefficients of carbon-dioxide gas at the turbulent free surface estimated in this study are in good agreement with the existing experimental and sea-measurement data.

2. Governing equations

The treatment of multi-phase flows in MARS (Kunugi, 1997) is based on an interface-capturing method which considers both liquid and gas flows as a single effective fluid with variable properties; the interface is captured as a region of a sudden change in fluid properties. This approach can be incorporated in a fully conservative form in the usual finite volume method. In addition to the following conservation equations for the mass and momentum, one has to solve an additional equation for the volume fraction of one phase, $F(t, x_i)$ as follows:

$$\langle F\rangle = \sum F_m, \tag{1}$$

where F_m denotes a volume fraction of the mth fluid and $\langle\ \rangle$ represents a spatial mean. One sets $F = 1$ for control volumes filled with liquid and $F = 0$ for gas.

In the present study, the following assumptions for deriving the governing equations are made: (1) Newtonian fluid is assumed, (2) thermal properties are kept constant and (3) thermal radiation and viscous dissipation can be neglected. The continuity equation for the multi-phase flows of m fluids can be expressed as

$$\frac{\partial F_m}{\partial t} + (U\cdot\nabla)F_m = \frac{\partial F_m}{\partial t} + \nabla\cdot(F_m U) - (F_m\cdot\nabla)U = 0. \tag{2}$$

The momentum equation with the continuum surface force (CSF) model proposed by Brackbill et al. (1992) can be written by

$$\frac{\partial U}{\partial t} + \nabla(UU) = G - \frac{1}{\langle\rho\rangle}\nabla P - \nabla\cdot\tau + \frac{1}{\langle\rho\rangle}F_v. \tag{3}$$

The CSF term, F_v at the certain surface position x_s can be modeled as

$$F_v(x_s) = [\sigma\kappa(x_s) + \tau_2(x_s)_{ii} - \tau_1(x_s)_{ii}]n(x_s)\langle\rho(x_s)\rangle/\bar{\rho}, \tag{4}$$

where σ is the surface tension coefficient, $\kappa(x_s)$ is the surface curvature at x_s and $n(x_s)$ is the normal vector to the surface at x_s. Other thermal properties, such as the mean density ρ, the mean viscosity μ and the viscous stress τ are defined by the following equations:

$$\begin{aligned}
&\langle\rho\rangle = \sum(F_m\rho_m), \quad \bar{\rho} = (\rho_g + \rho_l)/2,\\
&\langle\langle\phi\rangle\rangle = \left[\phi_g \times \left\{\mathrm{sign}\left(F_g - F_l\right) + 1\right\}\right.\\
&\qquad \left. + \phi_l \times \left\{1 - \mathrm{sign}\left(F_g - F_l\right)\right\}\right]/2,\\
&\tau = -[\langle\langle\mu\rangle\rangle/\langle\langle\rho\rangle\rangle]\left[I(\nabla U) + (\nabla U)^{\mathrm{T}}\right],
\end{aligned} \tag{5}$$

where the suffices, g and l, denote the gas and the liquid phases, respectively. ϕ is a general variable such as ρ and μ. Another average of properties at the free surface region is defined as $\langle\langle\phi\rangle\rangle$.

The momentum equation (3) can be solved by means of the well-known projection method (Chorin, 1968). The velocities at new time-step can be obtained by solving the Poisson equation of pressure. Then, a fluid volume flux per one time-step, δF can be calculated and transported by the multi-interfaces advection and reconstruction procedure, that is, the MARS (Kunugi, 1997). The accuracy of mass conservation for the gas–liquid interacting flow situation is around 0.001% in a million computation time-steps in case of a slug-plug flow analyses of stratified flows in a horizontal duct (Kunugi et al., 1999c).

The mass transport equation for the carbon-dioxide gas can be expressed as follows:

$$\frac{\partial}{\partial t}\langle\rho\rangle C + \nabla\cdot(\langle\rho\rangle CU) = \nabla\cdot(D\nabla C) + S, \tag{6}$$

where C is a concentration (i.e., mole fraction) of carbon-dioxide, D is a molecular diffusivity and S is an absorbed molar flux at the free surface based on the following Henry's law:

$$C_s = P_s/H, \tag{7}$$

where C_s is a saturated concentration at free surface corresponding to the saturation solubility, P_s is an instantaneous pressure at free surface and H is the Henry's constant corresponding to the pressure, P_s.

As for the discretization of the governing equations on the Cartesian coordinate system, the second-order scheme for the spatial differencing terms is used on the staggered grid system and the Euler implicit scheme is used for the first stage of projection method to solve the momentum equation. The gas absorption at free surface is treated as an internal boundary condition based on Eq. (7).

3. Problem description

The physical problem treated here is the motion of two Newtonian immiscible incompressible fluids, i.e., air and water, with the deformation of the interface between them. In Fig. 1, the problem schematic view is shown. Both gas- and liquid-flows flow in parallel. The computational domain is $W = 0.157$ m in width (z-direction), $2h = 0.05$ m in height (y-direction) and $L = 0.281$ m in length (x-direction). The periodic boundary conditions in the spanwise (z) and streamwise (x) directions are imposed and the free-slip boundaries are applied to both upper and lower boundaries in y-direction. The initial free surface is located at the mid-plane of the total height, i.e., $h = 0.025$ m. The bulk Reynolds number based on the gas layer height (h) and the free stream velocity U_∞ is $Re(= U_\infty h/\nu) = 3459$. The initial liquid velocity is assumed to be one-hundredth of the gas velocity in this study.

The number of the computational grids is 128 in z-direction (spanwise), 300 in y-direction (height) and 192 in x-direction (streamwise). The inclement of computational time-step is around 10^{-6} to 10^{-5} s depending on the cell Courant number and residuals of the mass conservation. In order to investigate the effect of grid refinement in y-direction on the turbulence statistics at the free surface, we carried out two grid systems with the same number of grids because of the limitation of the computer memory: (1) uniform grid spacing ($\Delta y = 167$ μm) and (2) non-uniform grid spacing ($\Delta y = 30$ μm: the closest grid to the free surface). According to the results of the grid refinement test, it is found that the significant imbalance of the turbulent energy budget at the free surface region was shown in case of uniform grid spacing. On the other hand, in case of non-uniform grid spacing the budget of turbulent kinetic energy seems to be reasonable as shown in Fig. 9. Therefore, the later non-uniform grid spacing is used in the present study.

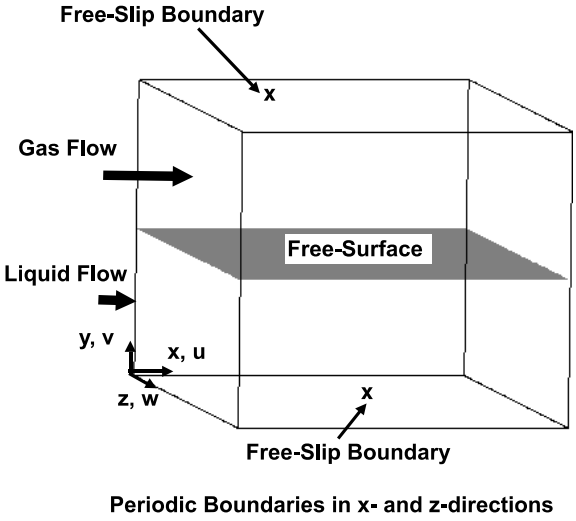

Fig. 1. Computational domain and boundary conditions.

4. Results and discussion

Fig. 2 shows a snapshot of the instantaneous flow visualization of the free surface behavior. The capillary wave motion can be observed in the streamwise direction. A few small dwells caused by a downdraft motion and droplet/bubble formation can be observed locally. The friction velocity in gas phase $u_{\tau(g)}$ is around 0.08 m/s and for the liquid phase $u_{\tau(l)}$ is around 0.02 m/s. These values are corresponding to the turbulent Reynolds number of gas phase, $Re_{\tau(g)} = 130$ and that of liquid phase, $Re_{\tau(l)} = 626$. The turbulence became weak at the early stage of computation because of relatively low $\mathrm{Re}_{\tau(g)}$, and then, it

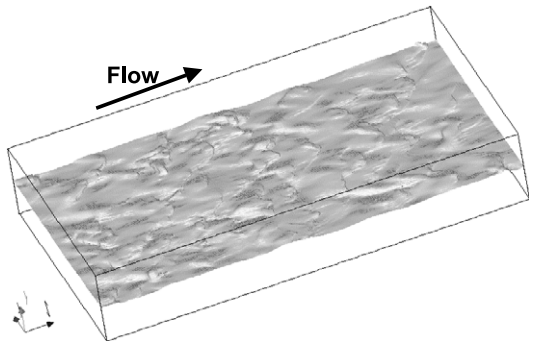

Fig. 2. A snapshot of the instantaneous flow visualization of the free surface behavior.

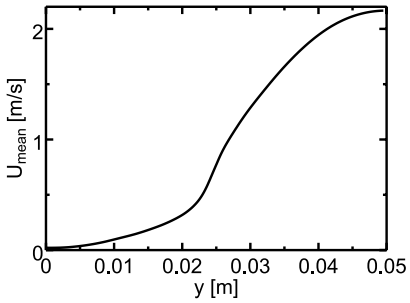

Fig. 3. Mean velocity distribution in y-direction ($y = 0.025$ m is the mean surface location).

recovered later due to the gas–liquid interaction: the liquid was driven by the shear wind and generated the high turbulence underneath the free surface. It can be considered that the turbulence interaction between gas and liquid flows at the free surface is very strong and important.

Fig. 3 shows the mean streamwise velocity distribution along y-axis. The liquid velocity near the bottom of the liquid region is kept small due to the hydrostatic pressure despite the free-slip condition imposed at the bottom boundary (see Fig. 5). It can be seen that the liquid velocity increases near the free surface. This shows that the momentum of the gas flow transports to the water due to the gas–liquid interaction at the free surface. At the ceiling of the solution domain, the gradient of mean velocity is almost zero, i.e., the mean velocity of the turbulent boundary layer flow reaches to the free stream velocity, U_∞.

In order to investigate the magnitude of the surface deformation, the mean free surface position, F_{mean} and the root-mean-square (rms) distributions of F are shown in Fig. 4. The mean surface wave fluctuation height δ is around ± 0.69 mm on the basis of the initial surface position. This result is close to the experimental data, around 1 mm ($= \pm 0.5$ mm) by Komori et al. (1989).

The mean pressure and the rms distributions of pressure fluctuation are shown in Fig. 5. It can be seen that the hydrostatic pressure forms in the liquid region and the maximum value of the rms distribution of pressure fluctuation is around 10% of the total hydrostatic pressure. This shows the very high turbulence that might be generating at the free surface region.

Fig. 6 shows the rms distributions of the velocity fluctuation in each direction. It can be seen that the peak rms values appear at the free surface region. The streamwise velocity fluctuation, u_{rms} shows the bigger peak than other two components because of two-dimensionality of this flow. The normal velocity fluctuation component, v_{rms}, is assumed to be zero in most turbulent open-channel flow studies. However, in the present study a large normal velocity fluctuation has been

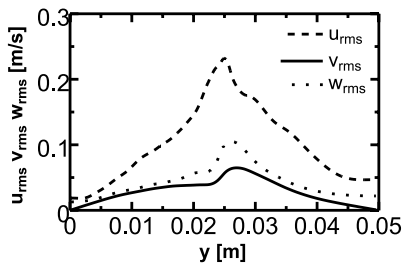

Fig. 4. Mean free surface distribution and rms distribution of free surface fluctuation.

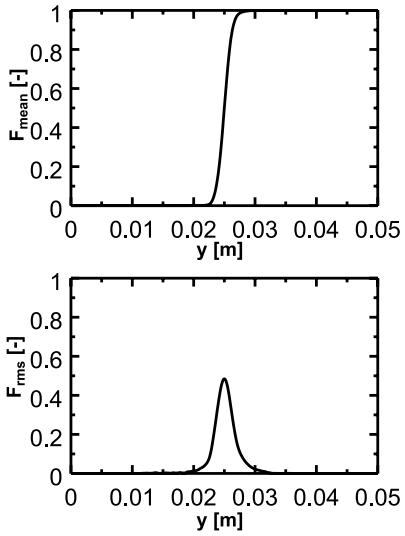

Fig. 5. Mean pressure distribution and rms distribution of pressure fluctuation.

generated at the free surface due to gas–liquid interaction. Judging from the rms distributions of the velocity fluctuation, these turbulent flows in both gas and liquid phases can be considered as a turbulent channel flow with a complete or incomplete wall.

Fig. 7 shows the two-point correlation function in the stream direction at three different heights: $y = 0.02$ m in the liquid region, $y = 0.025$ m at the free surface region and $y = 0.03$ m in the gas region. The correlation functions for three velocity components become zero in the downstream region. It shows that this flow has reached a fully developed state. According to the correlation function of normal velocity, it is found that the typical wavelength of the free surface is around 0.03 m and a little shorter than those of both gas and liquid phases. It is necessary to investigate the reason for this discrepancy by means of computational flow visualization techniques in the future.

Fig. 8 shows the energy spectra in streamwise direction versus wave number k_x at various heights: (a) $y = 0.02$ m, (b) 0.025 m and (c) 0.03 m. In the figures, E_{ii} denotes the energy spectra for velocity component, i, and E_F denotes for surface position and E_c for concentration. According to Fig. 8(b), the

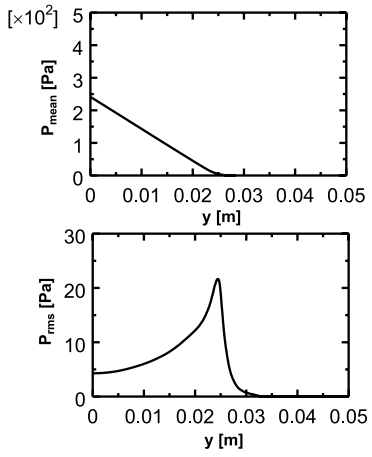

Fig. 6. Root mean square of velocity fluctuation distribution.

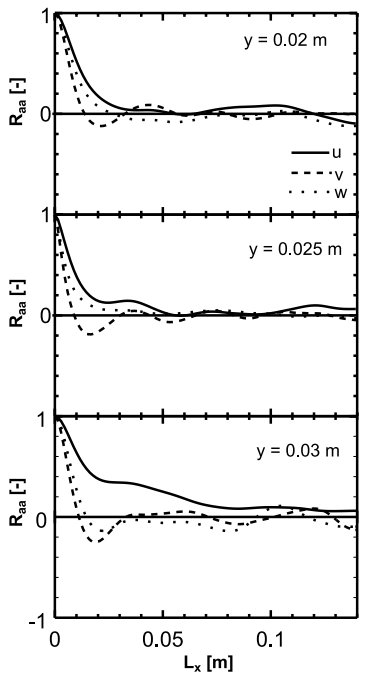

Fig. 7. Two-point correlation function in stream direction at three different heights.

slope of the spectra is close to $k^{-5/3}$. This means that the gas–liquid interaction of turbulent flow is dominant for generating turbulence in the free surface region. The slopes of spectra (k^{-4}) in both liquid and gas regions as shown in Fig. 8(a) and (c) are steeper than that at the free surface region. It means the turbulence flows in both gas and liquid phases away from the free surface have more dissipative features.

Fig. 9 shows the budget of turbulent kinetic energy. In the figure, a solid circle shows the turbulent production, a solid triangle shows the turbulent dissipation, an open diamond shows the viscous diffusion, a plus shows the pressure diffusion and an open square shows the turbulence diffusion term. A turbulent convection is almost zero all over the region, so it does not show in the figure. Turbulent production, turbulent dissipation, turbulent diffusion and pressure diffusion are large in the free surface region. It can be seen that the pressure diffusion is mainly balanced with turbulent dissipation. The viscous diffusion also varies in the free surface region, but the magnitude is small. Although the turbulent statistics can be obtained, it is difficult to discuss on the quantitative evaluation of the turbulence including gas–liquid interaction in the free surface region because of unsteady large density variation.

Fig. 10 shows the dimensionless mean streamwise velocity, U_{mean}/u_τ variation versus the distance from the free surface ($y/h = 0$ corresponds to the free surface and $y/h = 1$ to either boundary of gas or liquid phase), and also shows the comparison between the present DNS results and the experimental measurements by Nakayama and Nezu (2000). The solid line shows the present DNS for the liquid velocity and an open circle corresponds to the experimental results. The open triangle shows the experimental results for the gas velocity and the dashed line corresponds to the present DNS. Both results are fairly-good agreement with each other for both liquid and gas flows except the liquid velocity near free surface.

Fig. 11 shows the mean and rms concentration distributions. Although the molecular diffusivity D of carbon-dioxide to the air is five orders higher than that of aqueous carbon-dioxide to the water, the large mean and fluctuation of concentration appeared in both gas and liquid phases near the free surface. It can be considered that the turbulent mixing is enhanced by the gas–liquid interaction there.

Fig. 12 shows the gradients of the mean concentration distribution in each direction. The gradients in both spanwise and streamwise directions show small magnitude (10^{-2} to 10^{-1} m^{-1}) and have similar profiles because of the two-dimensionality of the flow. The gradient in normal direction to the free surface is four orders higher than those of other gradients and the peak value is around 5×10^2 m^{-1}.

Fig. 13 shows the mean correlation of velocity and concentration fluctuations along y-axis. All correlations show a similar tendency, however, the magnitudes of $\overline{v'c'}$ and $\overline{u'c'}$ are greater than $\overline{w'c'}$ at the free surface region.

From these results, the turbulent gas exchange coefficient can be estimated by using a turbulent diffusivity D_{turb} based on the following definition:

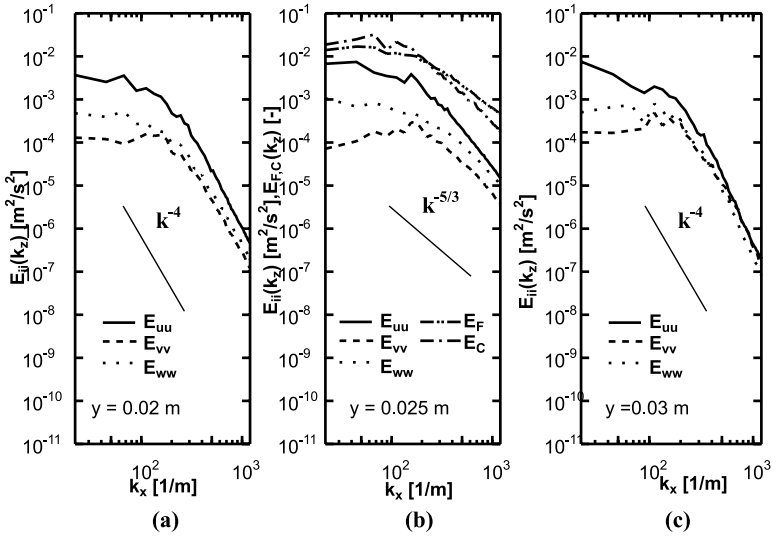

Fig. 8. Energy spectrum in streamwise direction for various heights.

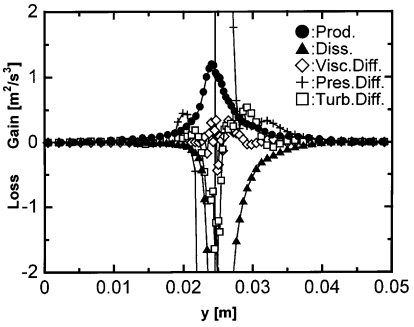

Fig. 9. Budget of turbulent kinetic energy.

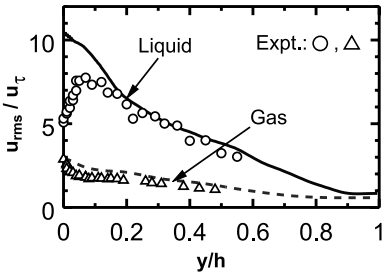

Fig. 10. Dimensionless mean streamwise velocity, U_{mean}/u_τ variation versus the distance from the free surface ($y/h = 0$ corresponds to the free surface and $y/h = 1$ to either boundary of gas or liquid phase).

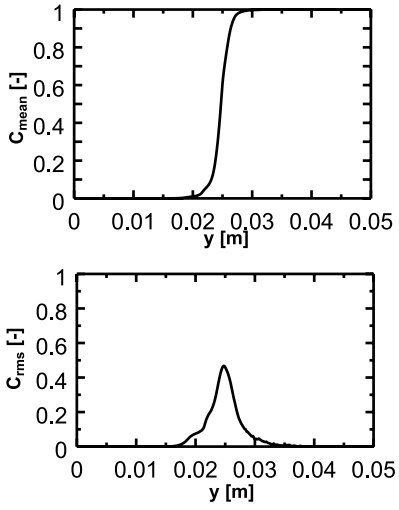

Fig. 11. Mean concentration distribution and rms distribution of concentration fluctuation.

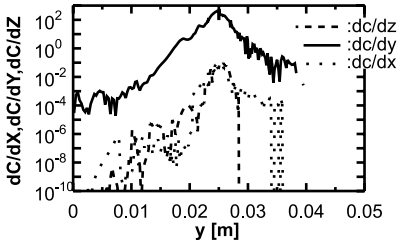

Fig. 12. Distributions of mean concentration gradient.

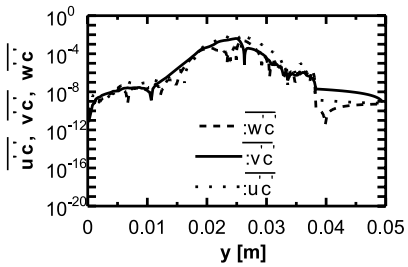

Fig. 13. Mean velocity-concentration correlation distributions along y-axis.

$$-\overline{v'c'} = D_{\text{turb}}\frac{\partial \overline{C}}{\partial y}, \tag{8}$$

where the over-bar denotes the average over the time and horizontal (x–z) plane. From the present DNS, it can be estimated that $D_{\text{turb}} = 1.5 \times 10^{-6}$ to 4×10^{-6} (m^2/s).

The turbulent exchange molar flux in y-direction, J can be calculated from the following mass transfer equation using a gradient of mean concentration and a turbulent gas exchange coefficient k_L:

$$J = -D\frac{\partial \overline{C}}{\partial y}, \tag{9}$$

$$J = k_L \Delta C. \tag{10}$$

Substituting Eq. (9) to Eq. (10), k_L can be obtained by

$$k_L = -D\frac{\partial \overline{C}}{\partial y}\Big/\Delta C, \tag{11}$$

where ΔC is the liquid concentration difference between the free surface region and the bottom boundary, i.e., $\Delta C = 0.33$–0.78. The turbulent gas exchange coefficient k_L can be estimated around 5×10^{-7} to 2×10^{-6} m/s and is almost the same order of the existing measuring data (Liss and Merlivat, 1986) as shown in Fig. 14. This higher diffusive region is being extended into the deeper liquid region due to turbulent mixing.

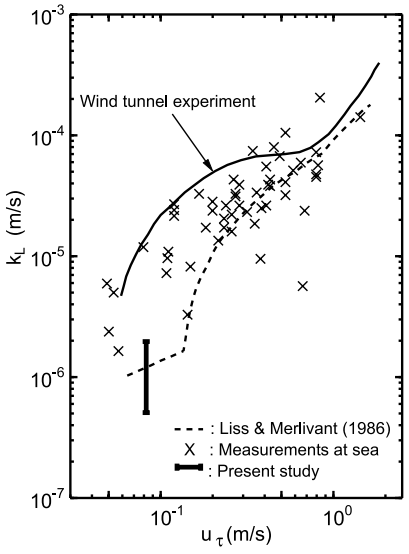

Fig. 14. Comparison of gas exchange coefficients between measuring data and the present DNS result.

5. Conclusion

The DNS for the turbulent free-surface flow with shear wind has been carried out by means of the coupled gas–liquid flow solution procedure, i.e., MARS method. From the present DNS results, the turbulent statistics for the free-surface characteristics are obtained and agree well with the experimental data (Nakayama and Nezu, 2000). It is found that the interaction between gas and liquid flows is very important for turbulent generation at the free surface due to shear wind. Henry's law can be used for the evaluation of a gas concentration at the free surface due to carbon-dioxide gas absorption. According to the concentration distribution of carbon-dioxide throughout both gas and liquid flow fields, a gas exchange coefficient of carbon-dioxide absorbed by water at the turbulent free surface is obtained and agrees well with the existing sea-measurement data (Liss and Merlivat, 1986). However, it should be necessary to investigate a more detailed mechanism of the gas absorption at liquid free surface caused by shear wind.

Acknowledgements

This work was supported by ACT-JST ('Research and development applying advanced computational science and technology' of Japan Science and Technology Corporation). The authors also acknowledge the Kansai Establishment of Japan Atomic Energy Research Institute for using the Fujitsu VPP300 vector-parallel supercomputer.

References

Angelis, V.D., Banerjee, S., 1999. Heat and mass transfer mechanisms at wavy gas–liquid interfaces. In: Banerjee, S., Eaton, J.K. (Eds.), Turbulence and Shear Flow Phenomena-1. Begell House, pp. 1249–1254.

Brackbill, J.U., Kothe, D.B., Zemach, C., 1992. A continuum method for modeling surface tension. J. Comput. Phys. 100, 335–354.

Chorin, A.J., 1968. Numerical solution of the Navier–Stokes equations. Math Comput. 22, 745–762.

Komori, S., Murakami, Y., Ueda, H., 1989. The relationship between surface-renewal and bursting motions in an open-channel flow. J. Fluid Mech. 203, 103–123.

Kunugi, T., 1997. Direct numerical algorithm for multiphase flows with free surfaces and interfaces. In: Proceedings of the ISAC'97 High Performance Computing on Multiphase Flows, JSME Centennial Grand Congress, pp. 25–30.

Kunugi, T., Satake, S., Ose, Y., 1999a. Direct numerical simulation on wave formation and breaking of turbulent free surface flow. In: Proceedings of the Second International Symposium on Two-Phase Flow Modelling and Experimentation, vol. 2, pp. 819–826.

Kunugi, T., Satake, S., Ose, Y., 1999b. Direct numerical simulation of turbulent free-surface flow. In: Banerjee S., Eaton, J.K. (Eds.), Turbulence ans Shear Flow Phenomena-1, Begell House Inc., pp. 621–626.

Kunugi, T., Ose, Y., Banat, M., 1999c. Slug-plug flow analyses of stratified flows in a horizontal duct by means of the MARS. In: Proceedings of the Fifth ASME/JSME Joint Thermal Engineering Conference, San Diego, USA, CD-ROM AJTE99-6435.

Liss, P.S., Merlivat, L., 1986. In: Buat-Menard, P. (Ed.), The Role of Air–Sea Exchange in Geochemical Cycling. Reidel, Dordrecht, pp. 113–127.

Lombardi, P., Angelis, V.D., Banerjee, S., 1996. Direct numerical simulation of near-interface turbulence in coupled gas–liquid flow. Phys. Fluids 8, 1643–1665.

Lam, K., Banerjee, S., 1992. On the condition of stream formation in a bounded turbulent flow. Phys. Fluid A 4, 306–320.

Nakayama, T., Nezu, I., 2000. Turbulence structure of wind water waves. J. Hydraulic Eng., JSCE, No.642/II-50, pp. 45–56 (in Japanese).

Rashidi, M., Banerjee, S., 1988. Turbulence structure in free surface channel flows. Phys. Fluids 31, 2491–2503.

Satake, S., Kunugi, T., 1998. Direct numerical simulation of an impinging jet into parallel disks. Int. J. Numer. Meth. Heat Fluid Flow 8, 768–780.

Tsai, W.-T., 1998. A numerical study of the evolution and structure of a turbulent shear layer under a free surface. J. Fluid Mech. 354, 239–276.